Article

Alfvénic velocity spikes and rotational flows in the near-Sun solar wind

https://doi.org/10.1038/s41586-019-1813-z

Received: 18 July 2019

Accepted: 17 October 2019

Published online: 4 December 2019

J. C. Kasper[1,2]*, S. D. Bale[3,4,5], J. W. Belcher[6], M. Berthomier[7], A. W. Case[2], B. D. G. Chandran[8,9], D. W. Curtis[4], D. Gallagher[10], S. P. Gary[11], L. Golub[2], J. S. Halekas[12], G. C. Ho[13], T. S. Horbury[5], Q. Hu[14], J. Huang[1], K. G. Klein[15,16], K. E. Korreck[2], D. E. Larson[4], R. Livi[4], B. Maruca[17,18], B. Lavraud[19], P. Louarn[19], M. Maksimovic[20], M. Martinovic[15], D. McGinnis[12], N. V. Pogorelov[14], J. D. Richardson[6], R. M. Skoug[11], J. T. Steinberg[11], M. L. Stevens[2], A. Szabo[21], M. Velli[22], P. L. Whittlesey[4], K. H. Wright[23], G. P. Zank[14], R. J. MacDowall[21], D. J. McComas[24], R. L. McNutt Jr[13], M. Pulupa[4], N. E. Raouafi[13] & N. A. Schwadron[8,9]

The prediction of a supersonic solar wind[1] was first confirmed by spacecraft near Earth[2,3] and later by spacecraft at heliocentric distances as small as 62 solar radii[4]. These missions showed that plasma accelerates as it emerges from the corona, aided by unidentified processes that transport energy outwards from the Sun before depositing it in the wind. Alfvénic fluctuations are a promising candidate for such a process because they are seen in the corona and solar wind and contain considerable energy[5–7]. Magnetic tension forces the corona to co-rotate with the Sun, but any residual rotation far from the Sun reported until now has been much smaller than the amplitude of waves and deflections from interacting wind streams[8]. Here we report observations of solar-wind plasma at heliocentric distances of about 35 solar radii[9–11], well within the distance at which stream interactions become important. We find that Alfvén waves organize into structured velocity spikes with duration of up to minutes, which are associated with propagating S-like bends in the magnetic-field lines. We detect an increasing rotational component to the flow velocity of the solar wind around the Sun, peaking at 35 to 50 kilometres per second—considerably above the amplitude of the waves. These flows exceed classical velocity predictions of a few kilometres per second, challenging models of circulation in the corona and calling into question our understanding of how stars lose angular momentum and spin down as they age[12–14].

The Parker Solar Probe (PSP) launched in August 2018 on a Delta IV Heavy rocket. The high energy of the launch, combined with a gravitational assist from Venus in September 2018, placed PSP into an eccentric orbit with a period of 147 days and a perihelion at a heliocentric distance of $r = 35.7R_\odot$ ($R_\odot$, solar radius) nearly a factor of two closer to the Sun than any previous mission[4]. This study uses observations made by instruments on the spacecraft during the first two encounters with the Sun, in November 2018 and April 2019. Whereas the instruments collect data at a low rate far from the Sun, the primary science collection at a high rate occurs during the encounter phase of each orbit at $r < 54R_\odot$ (0.25 AU). Encounter one (E1) lasted from 31 October to 12 November 2018, with the first perihelion occurring at 03:27 UT on 6 November. During these two encounters the longitude of PSP relative to the rotating surface of the Sun barely changed; PSP essentially dove down into, and then rose straight up from, a single narrow region above the Sun. E1 and E2 data thus describe a handful of specific solar-wind streams.

Nearly two million thermal-energy distribution functions of the solar-wind protons were recorded during E1, and more than three times that number during E2 (Fig. 1, Extended Data Fig. 1). From these distribution functions, the bulk properties of solar-wind protons—such as the velocity, density and temperature—are derived. Within any hour interval, the distribution of the radial solar-wind speed, V_{pR}, was strongly peaked at a

[1]Climate and Space Sciences and Engineering, University of Michigan, Ann Arbor, MI, USA. [2]Smithsonian Astrophysical Observatory, Cambridge, MA, USA. [3]Physics Department, University of California, Berkeley, CA, USA. [4]Space Sciences Laboratory, University of California, Berkeley, CA, USA. [5]The Blackett Laboratory, Imperial College London, London, UK. [6]Kavli Center for Astrophysics and Space Sciences, Massachusetts Institute of Technology, Cambridge, MA, USA. [7]Laboratoire de Physique des Plasmas, CNRS, Sorbonne Université, Ecole Polytechnique, Observatoire de Paris, Université Paris-Saclay, Paris, France. [8]Department of Physics and Astronomy, University of New Hampshire, Durham, NH, USA. [9]Space Science Center, University of New Hampshire, Durham, NH, USA. [10]Heliophysics and Planetary Science Branch ST13, Marshall Space Flight Center, Huntsville, AL, USA. [11]Los Alamos National Laboratory, Los Alamos, NM, USA. [12]Department of Physics and Astronomy, University of Iowa, IA, USA. [13]Johns Hopkins University Applied Physics Laboratory, Laurel, MD, USA. [14]Department of Space Science and Center for Space Plasma and Aeronomic Research, University of Alabama in Huntsville, Huntsville, AL, USA. [15]Lunar and Planetary Laboratory, University of Arizona, Tucson, AZ, USA. [16]Department of Planetary Sciences, University of Arizona, Tucson, AZ, USA. [17]Department of Physics and Astronomy, University of Delaware, Newark, DE, USA. [18]Bartol Research Institute, University of Delaware, Newark, DE, USA. [19]Institut de Recherche en Astrophysique et Planétologie, CNRS, UPS, CNES, Université de Toulouse, Toulouse, France. [20]LESIA, Observatoire de Paris, Université PSL, CNRS, Sorbonne Université, Université de Paris, Meudon, France. [21]NASA/Goddard Space Flight Center, Greenbelt, MD, USA. [22]Department of Earth, Planetary and Space Sciences, University of California, Los Angeles, CA, USA. [23]Universities Space Research Association, Science and Technology Institute, Huntsville, AL, USA. [24]Department of Astrophysical Sciences, Princeton University, Princeton, NJ, USA. *e-mail: jckasper@umich.edu

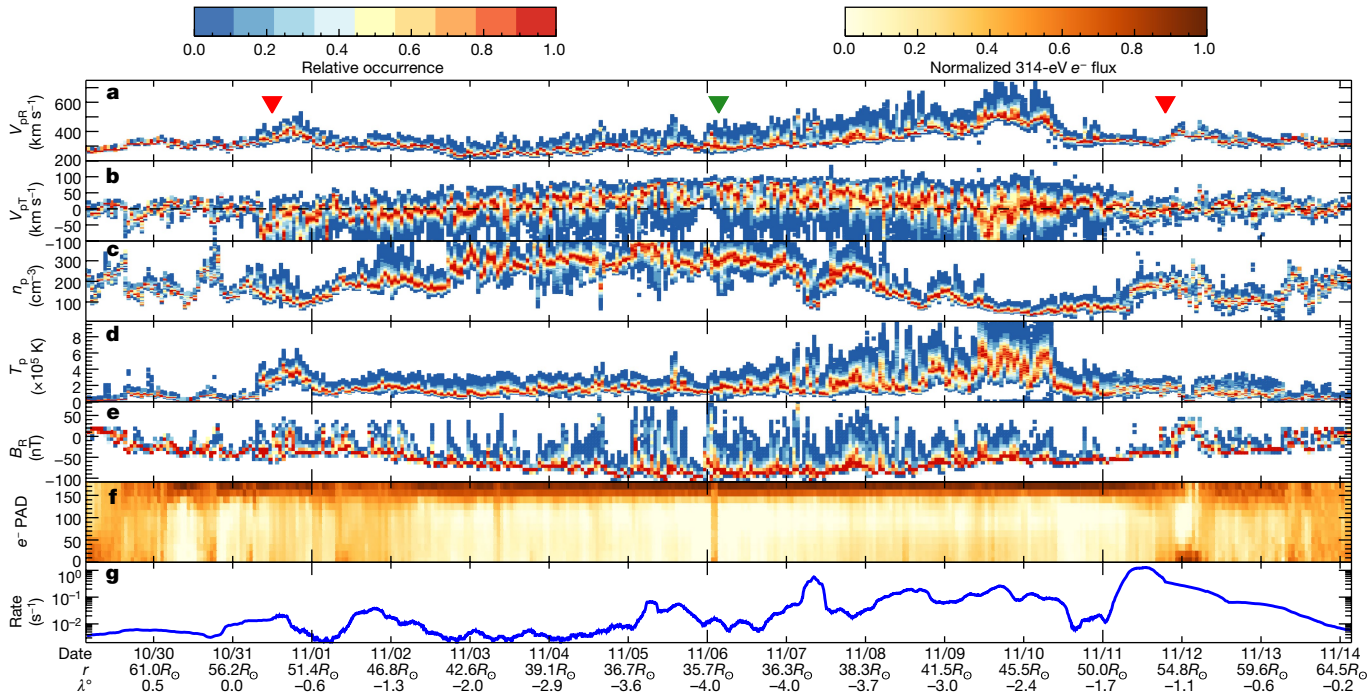

Fig. 1 | Overview of the first encounter of PSP with the Sun. a, Relative occurrence rate of the proton radial speed V_{pR} in one-hour intervals. Red triangles show the start and end of the high-rate data collection below $54R_\odot$ and the green triangle indicates a perihelion at $35.7R_\odot$. **b**–**f**, The same for V_{pT} in the solar equatorial plane (**b**), the proton number density n_p (**c**), the proton temperature T_p (**d**), the radial component of magnetic field B_R (e), the electron pitch-angle distribution (PAD) (**f**) and the 20–200 keV proton rate (**g**). The date (month/day), distance r and latitude λ relative to the solar equator are indicated at daily intervals.

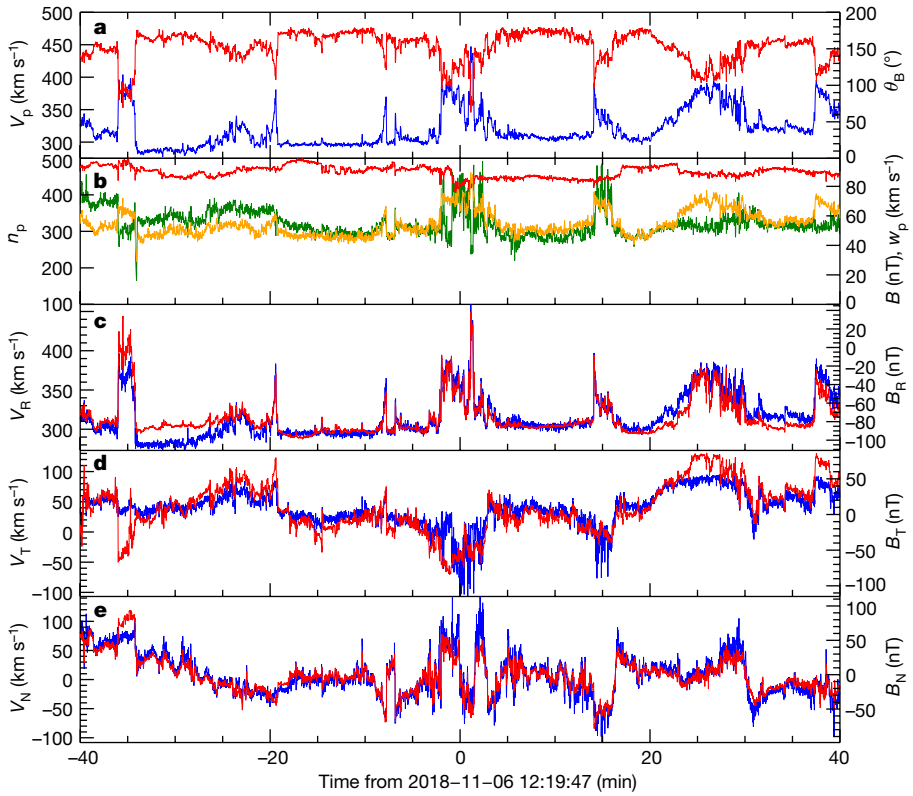

Fig. 2 | Solar-wind fluctuations near the closest approach. Near-Sun fluctuations meet the Alfvénic criteria, but are organized into structures and contain density enhancements. **a**, Magnitude of V_{pR} (blue) and angle θ_B of **B** from the radial direction outwards. **b**, Magnitudes of n_p (green), B (red) and the proton thermal speed w_p (yellow). **c**–**e**, Variation of each vector component of the velocity (blue) and magnetic field (red) in the radial direction (R), the transverse direction in the solar equatorial plane (T) and the normal to R and T (N). Since the orbit of PSP is within a few degrees of the solar equator, N points approximately north, perpendicular to the equatorial plane. There is a baseline solar-wind speed of about 300 km s^{-1} and jets where V_p jumps by about 100 km s^{-1}. The fluctuations are highly Alfvénic, with equal energy in the field and the flow, but they are organized into structures instead of being randomly distributed, and there is evidence of compressions.

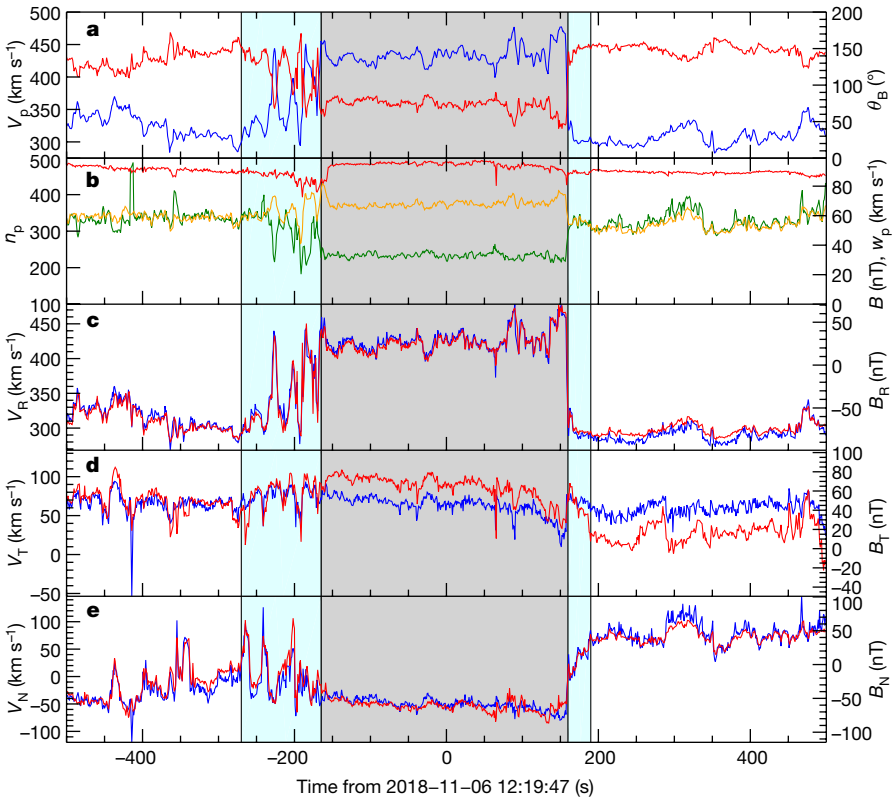

Fig. 3 | A closer look at a velocity spike. The formatting is as in Fig. 2, but focused on a single 1,000-s interval. The left blue region indicates the 105-s period in which PSP moved from the ambient plasma into the spike. The central core of the spike is indicated by the grey region and lasted for 325 s; it is characterized by a steady but disturbed flow and a field with a large rotation in **B** to $\theta_B \approx 70°$ and a jump in flow to 343 km s^{-1}. The return from the core spike into ambient solar wind is marked by the second blue region and lasted 30 s.

minimum value, with a one-sided tail extending to larger V_{pR} values. V_{pR} reached its minimum of 200 km s^{-1} about a quarter of the way though E1 and then rose steadily to about 600 km s^{-1}. Numerical simulations and simple extrapolations of the observed photospheric magnetic field suggest that PSP spent all of E1 south of the global heliospheric current sheet, in a region with inward magnetic polarity ($B_R < 0$)[15]. Near the start and end of E1, PSP sampled slow wind from near the global heliospheric current sheet. Closer to the Sun, PSP first observed very slow wind and then fast wind, both of which are thought to emerge from a low-latitude coronal hole[15]. Below 40$R_\odot$, V_{pT} (the transverse component of the proton velocity in the equatorial plane of the Sun) has a net positive value, which peaks at the closest approach. This flow may be the long-sought signature of plasma co-rotation in the corona. The density peaks in the slowest wind, at a value of approximately 400 cm^{-3}, about 50 times higher than values typically observed at 1 AU, as expected from mass conservation and spherical expansion. The proton temperature, T_p, and V_{pR} remain positively correlated[16]. At perihelion the protons are about 4 times hotter than protons with similar V_{pR} at 1 AU, consistent with radial scalings reported from earlier missions[4]. The radial component of the magnetic field, B_R, increases in magnitude with proximity to the Sun but unexpectedly changes sign many times. The pitch-angle (θ) distribution for electrons (that is, the number of electrons at a given energy as a function of their angle relative to **B**) is a valuable diagnostic of these changes in the direction of **B**. Here we show the pitch-angle distribution in a 22-eV-wide energy channel centred on 314 eV, well above the electron thermal energy. The sharp peak near 180° corresponds to the strahl, a beam of super-thermal electrons that travel away from the Sun along magnetic-field lines. Near the Sun, the strahl evolves towards small sinθ values because of magnetic-moment conservation[17]. If the reversals in B_R seen by PSP result from the spacecraft's crossing between open field lines (connected to the Sun at only one end) with different signs of B_R back at the Sun, then the strahl would flip between 180° and 0° each time B_R changed sign. Instead, every time B_R flips, the strahl maintains its 180° orientation, clearly indicating that the reversals in B_R are due to S-like bends in the magnetic-field lines (Extended Data Fig. 2). Closed field lines with both ends connected to the Sun and strahl travelling in both parallel and antiparallel directions to **B** are seen during the arrival of a coronal mass ejection on 11 November at 23:50 UT, following an enhancement in the number of energetic particles[18].

Figure 2 shows a timeseries of 80 min of observations several hours after perihelion, illustrating typical velocity and magnetic-field fluctuations. About half the time, **B** points radially inwards towards the Sun and the velocity V remains at a relatively constant 300 km s^{-1}. The remaining time includes seven distinct intervals in which **B** rotates away from its radial–inward orientation, V_{pR} simultaneously jumps and **V** also rotates, linking the one-sided tail in V_{pR} with the reversals in polarity seen in the E1 overview. These jumps in flow associated with rotations in **B** and **V** are similar to one-sided Alfvénic structures that were first seen farther from the Sun[6,7]. The spikes seen by PSP are different in that they have larger amplitudes and are often associated with an increase in the proton density, n_p, indicating that the spikes have a non-Alfvénic component. The correlated variations in the components of B and V, their relative amplitudes and the constant value of |**B**| are consistent with large-amplitude, spherically polarized Alfvén waves propagating through the plasma in the anti-Sunward direction, similar to earlier observations[5,19]. We can classify this wind stream (and indeed much of E1) as Alfvénic slow solar wind[20].

About 1,000 long-duration (>10 s) and isolated velocity spikes with large rotations in **B** were identified in E1 (about half as many were seen in E2.) Often the spikes can be separated chronologically into a core region with plasma conditions that are very different from those of the ambient solar wind but relatively constant, a comparatively short

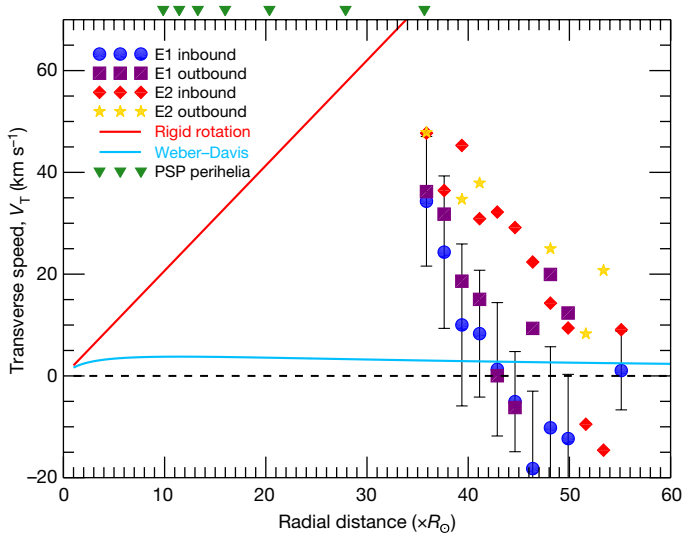

Fig. 4 | Large circulation of solar wind observed near the Sun. Averaged rotational (or azimuthal) flow, V_{pT}, over 1.75$R_\odot$ intervals during E1 (inbound in blue, with error bars indicating the standard deviation from all observations; outbound in purple) and E2 (inbound in red; outbound in yellow) as a function of radial distance. Each symbol represents the average over at least 10,000 observations, and the values closest to perihelion are averaged over 60,000–230,000 observations. Error bars for E1 inbound show one standard deviation of the individual observations and are representative of the variation for the other three phases. The uncertainty in the mean of V_{pT} is much smaller than the marker size. Current and upcoming perihelia are shown with green triangles. Lines indicate no rotation (dashed), rigid co-rotation everywhere (red) and the axisymmetric Weber–Davis model (blue).

transition region on one side of the core, and a longer transition region on the other side containing large-amplitude fluctuations (see Fig. 3). During the 105-s transition at the beginning of this spike, the flow underwent seven large oscillations with an amplitude of 150 km s^{-1}, which possibly resulted from a Kelvin–Helmholtz instability.

Equally unexpected as the spikes and B_R reversals are the large-amplitude and sustained positive rotational velocities seen below 40$R_\odot$ for E1 and 50$R_\odot$ for E2 (Fig. 4). Net rotation has been reported farther from the Sun, but it was of the same order as instrument error and much smaller than the standard deviation in flow due to fluctuations and stream interactions[8,21]. Here V_{pT} rises to 35 km s^{-1} (E1) and 50 km s^{-1} (E2). This is much greater than the variance from fluctuations including the velocity spikes, there is no evidence of stream interactions, and these values are much greater than the precision in the averaged flows (less than 0.5 km s^{-1}) and the absolute error in the flow due to a pointing error (less than 3 km s^{-1}) (see Methods). These are the first in situ observations of net rotational flow in the solar wind that are significantly above fluctuations and uncertainty.

Some level of rotational flow has always been expected in the solar wind near the Sun, as magnetic tension in the corona should force the plasma to rotate as the Sun spins. However, the large rotational velocities measured here greatly exceed the value calculated by the axisymmetric Weber–Davis model[13], posing a major challenge to our understanding of the dynamics of the near-Sun solar wind. Determining the origin of these tangential flows will be essential for understanding how the Sun loses angular momentum and spins down as it ages[12,14,22]. Further studies of the angular momentum should include magnetic fields, waves and different ions. Future PSP orbits will clarify the extent to which these large rotational flows characterize other solar-wind streams. These orbits will also provide critical additional diagnostics of the state of the plasma, including turbulence, velocity spikes, temperature anisotropy and particle velocity distribution functions, at heliocentric distances as small as 9.86$R_\odot$.

Online content

Any methods, additional references, Nature Research reporting summaries, source data, extended data, supplementary information, acknowledgements, peer review information; details of author contributions and competing interests; and statements of data and code availability are available at https://doi.org/10.1038/s41586-019-1813-z.

1. Parker, E. N. Dynamics of the interplanetary gas and magnetic fields. *Astrophys. J.* **128**, 664–676 (1958).
2. Gringauz, K. I., Bezrokikh, V. V., Ozerov, V. D. & Rybchinskii, R. E. A study of the interplanetary ionized gas, high-energy electrons and corpuscular radiation from the Sun by means of the three-electrode trap for charged particles on the second Soviet cosmic rocket. *Sov. Phys. Dokl.* **5**, 361–364 (1960).
3. Bonetti, A., Bridge, H. S., Lazarus, A. J., Rossi, B. & Scherb, F. Explorer 10 plasma measurements. *J. Geophys. Res.* **68**, 4017–4063 (1963).
4. Marsch, E. et al. Solar wind protons – three-dimensional velocity distributions and derived plasma parameters measured between 0.3 and 1 AU. *J. Geophys. Res.* **87**, 52–72 (1982).
5. Belcher, J. W. & Davis, L. Jr Large-amplitude Alfvén waves in the interplanetary medium, 2. *J. Geophys. Res.* **76**, 3534–3563 (1971).
6. Gosling, J. T., McComas, D. J., Roberts, D. A. & Skoug, R. M. A one-sided aspect of Alfvenic fluctuations in the solar wind. *Astrophys. J. Lett.* **695**, 213–216 (2009).
7. Horbury, T. S., Matteini, L. & Stansby, D. Short, large-amplitude speed enhancements in the near-Sunfast solar wind. *Mon. Not. R. Astron. Soc.* **478**, 1980–1986 (2018).
8. Pizzo, V. et al. Determination of the solar wind angular momentum flux from the HELIOS data – an observational test of the Weber and Davis theory. *Astrophys. J.* **271**, 335–354 (1983).
9. Fox, N. J. et al. The solar probe plus mission: humanity's first visit to our star. *Space Sci. Rev.* **204**, 7–48 (2016).
10. Kasper, J. C. et al. Solar Wind Electrons Alphas and Protons (SWEAP) investigation: design of the solar wind and coronal plasma instrument suite for Solar Probe Plus. *Space Sci. Rev.* **204**, 131–186 (2016).
11. Bale, S. D. et al. The FIELDS instrument suite for Solar Probe Plus. Measuring the coronal plasma and magnetic field, plasma waves and turbulence, and radio signatures of solar transients. *Space Sci. Rev.* **204**, 49–82 (2016).
12. Schatzman, E. A theory of the role of magnetic activity during star formation. *Ann. d'Astr.* **25**, 18–29 (1962).
13. Weber, E. J. & Davis, L. Jr The angular momentum of the solar wind. *Astrophys. J.* **148**, 217–227 (1967).
14. Finley, A. J., Matt, S. P. & See, V. The effect of magnetic variability on stellar angular momentum loss. I. The solar wind torque during sunspot cycles 23 and 24. *Astrophys. J.* **864**, 125 (2018).
15. Bale, S. D. et al. Highly structured slow solar wind emerging from an equatorial coronal hole. *Nature* https://doi.org/10.1038/s41586-019-1818-7 (2019).
16. Elliott, H. A., Henney, C. J., McComas, D. J., Smith, C. W. & Vasquez, B. J. Temporal and radial variation of the solar wind temperature–speed relationship. *J. Geophys. Res. Space Phys.* **117**, A09102 (2012).
17. Pilipp, W. G. et al. Characteristics of electron velocity distribution functions in the solar wind derived from the helios plasma experiment. *J. Geophys. Res. Space Phys.* **92**, 1075–1092 (1987).
18. McComas, D. M. et al. Probing the energetic particle environment near the Sun. *Nature* https://doi.org/10.1038/s41586-019-1811-1 (2019).
19. Vasquez, B. J. & Hollweg, J. V. Formation of arc-shaped Alfvén waves and rotational discontinuities from oblique linearly polarized wave trains. *J. Geophys. Res.* **101**, 13527–13540 (1996).
20. Bruno, R. & Carbone, V. The solar wind as a turbulence laboratory. *Living Rev. Sol. Phys.* **10**, 2 (2013).
21. Richardson, I. G. Solar wind stream interaction regions throughout the heliosphere. *Living Rev. Sol. Phys.* **15**, 1 (2018).
22. Axford, W. I. The solar wind. *Sol. Phys.* **100**, 575–586 (1985).

Methods

Data collection and analysis

The data presented here were collected over the course of the first two encounters of the Sun by PSP in November 2018 and April 2019. This study makes use of all of the in situ instruments on the spacecraft. The thermal plasma properties are measured by the PSP SWEAP (Solar Wind Electrons Alphas and Protons) instrument suite[10], including the Solar Probe Cup (SPC) and the Solar Probe Analyzers (SPAN) for electron and ion plasma data. Magnetic-field data from the outboard FIELDS magnetometer were also used[11,15], along with energetic-particle rates as seen by IS⊙IS[18]. SPC measures the reduced distribution function of ionized hydrogen and helium and the two-dimensional flow angles of the ions as a function of energy/charge. These measurements were performed at least once per second and typically more than four times per second throughout the encounter phase of each orbit (below 0.25 AU or $54R_\odot$). This paper uses moments of the entire SPC proton distribution function to calculate the total effective proton velocity, density and radial component of the temperature. While the SPAN ion sensor generally did not view the peak of the proton velocity distribution, the overlapping regions seen by SPAN and SPC were compared to confirm that there were no gross offsets in the calibration or the derived plasma properties such as the velocity; this technique will be more accurate when the solar wind flows into SPAN closer to the Sun. Observations of electrons with a central energy of 314 eV and a width of 22 eV by the two SPAN electron sensors were combined, along with the FIELDS determination of the magnetic-field direction, to create the electron pitch-angle distributions.

All data are being archived and will be available for download at the NASA Space Physics Data Facility in November 2019 (https://spdf.gsfc.nasa.gov/). Additional SWEAP data and information are available at the SWEAP web page (http://sweap.cfa.harvard.edu/). Data were analysed and graphics were developed in IDL (Interactive Data Language).

Statistics

The distributions of plasma properties in Fig. 1 and Extended Data Fig. 1 were produced with a time resolution of 1 h. During the encounters, the time resolution of the plasma instrument ranged from slightly more than one measurement per second to more than four measurements per second, so each column represents the distribution of approximately 3,600–14,400 measurements. All error bars indicate one standard deviation of the measurements from the mean. At least 10,000—and generally more than 80,000—observations were used to calculate the mean transverse flow V_{pT} in Fig. 4.

Estimates of uncertainty

Here we discuss the absolute accuracy of SPC ion measurements. As verified by ground testing, the absolute accuracy for V_{pR} is less than 0.01% over a measurable range of approximately 119 km s^{-1} to 1,065 km s^{-1}. The absolute accuracy in temperature is similarly small over a measurable range of approximately 7.3 kK to 21.1 MK (that is, proton thermal speeds of 11 km s^{-1} to 600 km s^{-1}). Speeds and temperatures at the extremes of these ranges are subject to systematic considerations, but no such measurements are presented here. The accuracy of the density measurement is determined by comparison with the plasma frequency as observed by FIELDS[11]. Thus, the absolute accuracy of the SPC density measurement is estimated to be about 1% and is no worse than 3%. The absolute accuracy for off-radial flow components is verified via spacecraft roll manoeuvres about the SPC symmetry axis. For solar-wind fluxes typical of the first two encounters, the uncertainty associated with this calibration corresponds to a typical absolute accuracy of about 0.5°. For a solar wind of 400 km s^{-1} this corresponds to an expected error in V_{pT} of 3–4 km s^{-1}, which is much smaller than the net rotational flow observed.

Signatures of Alfvénic fluctuations

In discussing Fig. 2, we stated that the correlation of fluctuations in the components of **B** and **V** were generally indicative of outward-propagating Alfvén waves. We consider the vector waves or fluctuations $\Delta\mathbf{V}$ and $\Delta\mathbf{B}$ superimposed on a steady background of $\mathbf{B}_o$ and $\mathbf{V}_o$, respectively. In the long-wavelength fluid magnetohydrodynamic limit, Alfvén waves propagate exactly in parallel or antiparallel directions to $\mathbf{B}_o$, are dispersionless and do not compress the plasma, and there is a simple linear relationship of $\Delta\mathbf{B} = \pm D_A\Delta\mathbf{V}$, where $D_A = (n_p + 4n_\alpha)^{0.5}\Theta/21.8$ (in units of nT km^{-1} s; densities are in units of cm^{-3}) and $\Theta = (1-\beta_\parallel+\beta_\perp)^{-0.55}$. Here Θ is a correction for thermal pressure anisotropy, where $\beta_\parallel$ is the ratio of the parallel plasma pressure to the magnetic pressure and $\beta_\perp$ is the ratio of the perpendicular plasma pressure to the magnetic pressure. For this period we find on average $n_p = 220$ cm^{-3}, $\beta_\parallel = 0.202$ and $\beta_\perp = 0.315$. SPC and SPAN were not configured optimally to measure the ionized helium abundance n_α, so assuming the typical range $0.5\% < n_\alpha/n_p < 4.5\%$, we expect $D_A = 0.68$–0.74 nT km^{-1} s. We find D_A for the R, T, N components to be 0.71, 1.09 and 0.70 nT km^{-1} s, respectively, so the R and N components are exactly within the expected range and the fluctuations in the T direction are about 33% higher (it is typical for D_A to be different for each component of the velocity[5]). We then used the calculated value of D_A to rescale the range of the vector components of **B**, so they should overlap with **V** if the fluctuations were purely Alfvénic. The sign of the relation between $\Delta\mathbf{B}$ and $\Delta\mathbf{V}$ is given by the sign of $-\mathbf{k}\cdot\mathbf{B}_o$, where **k** is the wavevector and gives the direction of propagation, and **B** is an average direction of the field over a long time scale. The ambient direction of the magnetic field outside the large-amplitude fluctuations points towards the Sun and the correlations are overwhelmingly positive, meaning that we are seeing outward-propagating waves.

Identification of velocity spikes

Isolated velocity spikes were identified by looking for all intervals in each encounter in which the orientation of the magnetic field started in the quiet configuration pointed towards the Sun within 30°, rotated more than 45° away from the quiet configuration for at least 10 s, and then returned to the original direction. Candidate events were then examined manually to identify starting and ending times.

Acknowledgements The SWEAP Investigation and this study are supported by the PSP mission under NASA contract NNN06AA01C. The SWEAP team expresses its gratitude to the scientists, engineers and administrators who have made this project a success, both within the SWEAP institutions and from NASA and the project team at JHU/APL. J.C.K. acknowledges support from the 2019 Summer School at the Center for Computational Astrophysics, Flatiron Institute. The Flatiron Institute is supported by the Simons Foundation. S.D.B. acknowledges the support of the Leverhulme Trust Visiting Professorship programme. T.S.H. was supported by UK STFC ST/S0003641/1.

Author contributions J.C.K. is the SWEAP Principal Investigator (PI) and led the data analysis and writing of this Article. S.D.B. is the FIELDS PI and a SWEAP Co-Investigator and provided the magnetic-field observations. J.W.B. leads the US group that developed the solar-wind Faraday cup, and provided guidance on identifying Alfvénic fluctuations. M.B. provided a pre-amplifier ASIC used within the SPAN electron instruments. A.W.C. is the SPC instrument scientist and ensured that the instrument met its performance requirements and was calibrated. B.D.G.C. contributed to the theoretical calculations and the writing of the manuscript. D.W.C. managed the effort at UCB. D.G. was the institutional lead at NASA MSFC, responsible for materials testing and calibration of SPC. S.P.G. provided recommendations on measurement requirements to detect instabilities. L.G. provided related solar observations and results. J.S.H. contributed to the analysis of the electron observations and to the writing of the manuscript. G.C.H. provided a time-of-flight ASIC to reduce the size and power of the SPAN ion instrument. T.S.H. participated in the analysis of the Alfvénic spikes. Q.H. identified magnetic flux ropes. K.G.K. contributed to the writing of the manuscript and provided warm-plasma growth rate calculations. K.E.K. led the SWEAP Science Operations Center and coordinated observing plans between the instruments and the project. M.V. contributed to the writing of the manuscript and the discussion on the relationship between Alfvénic fluctuations and angular momentum. D.E.L. is the institutional lead at Berkeley, responsible for the implementation of the SPAN instruments and the SWEAP Electronics Module suite-wide computer. R.L. is the SPAN ion instrument scientist. B.L. identified flux ropes and other signatures of coronal mass ejections in the data. P.L. coordinated solar furnace testing of the SPC materials before launch. M. Maksimovic peformed the absolute calibration of the density measurements. M. Martinovic evaluated the quality of the velocity distribution functions. N.V.P. carried out numerical

simulations. J.D.R. contributed to the design of the Faraday cup. R.M.S. helped to interpret the electron pitch-angle distributions. J.T.S. identified potential field rotation causes. M.L.S. provided the overall data pipeline for SWEAP and SPC high-level data products. A.S. estimated the location of the heliospheric current sheet. P.L.W. set up the SPC calibration at MSFC and then became SPAN electron instrument scientist at Berkeley. K.H.W. arranged the SPC calibration at MSFC. G.P.Z. leads the SWEAP theory team. R.J.M. leads the FIELDS fluxgate magnetometer. D.J.M. is the IS⊙IS PI and provided the energetic-particle data. R.L.M. leads the EPI-Lo energetic-particle instrument. M.P. is the FIELDS SOC lead. N.E.R. is the PSP Project Scientist and reviewed jets and similar coronal transients. N.A.S. runs the IS⊙IS Science Operations Center. All authors participated in planning the observations and data collection, reviewed and discussed the observations, and read, provided feedback and approved the contents of the manuscript.

Competing interests The authors declare no competing interests.

Additional information

Correspondence and requests for materials should be addressed to J.C.K.

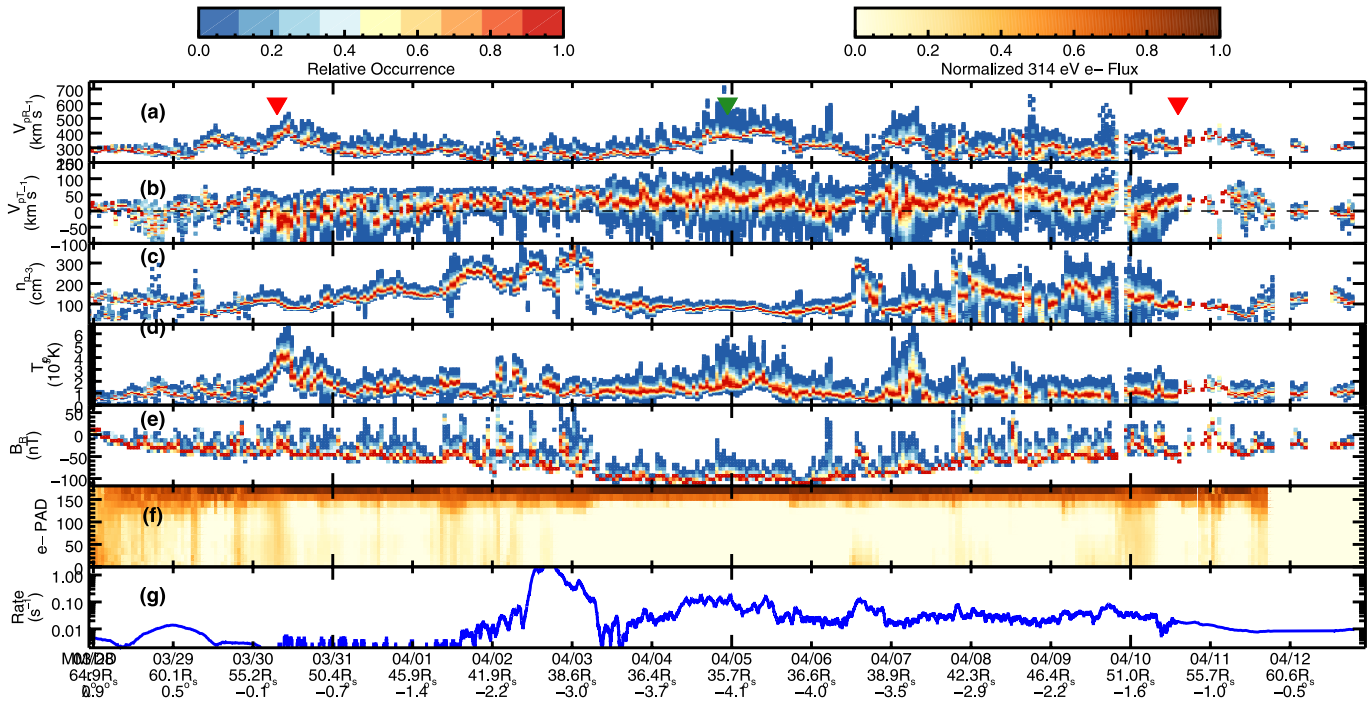

Extended Data Fig. 1 | Overview of the second PSP encounter with the Sun. The figure is in the same format as Fig. 1. Spikes in the velocity are again seen to be coincident with the magnetic-field reversals, but the jump in the speed is smaller, probably because the Alfvén speed was lower in E2 than E1. The density at perihelion is substantially lower.

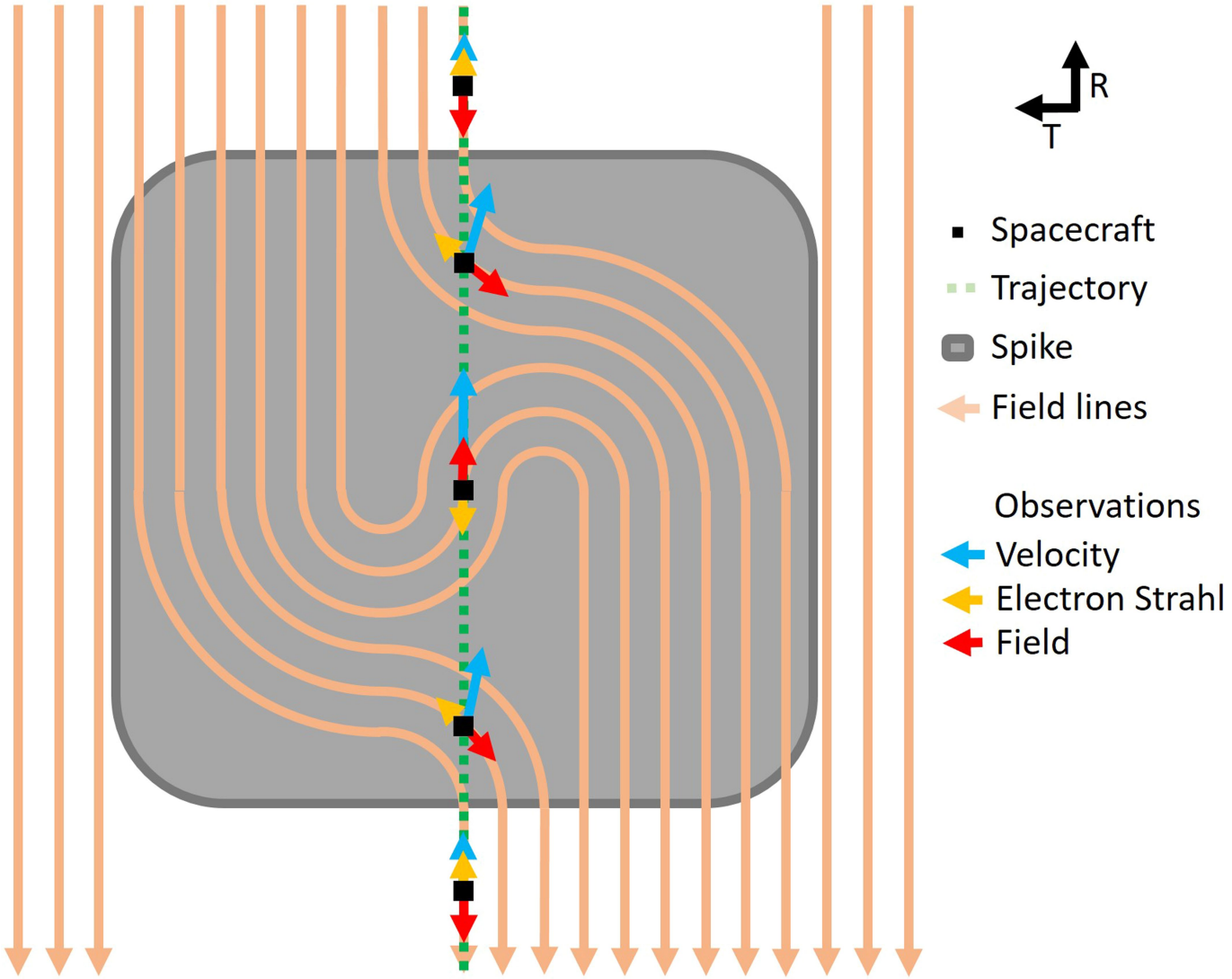

Extended Data Fig. 2 | Schematic of an S-shaped magnetic structure creating a field reversal, heat-flux reversal and a spike in velocity. This figure illustrates the possible geometry of an S-shaped propagating Alfvénic disturbance (grey box) and how it would appear to the spacecraft (black square) as it flew through the spike on the green trajectory. The pink lines with arrows indicate the configuration of the magnetic field, with all field lines ultimately pointing back to the Sun. Arrows at each black square indicate the vector velocity (blue), electron strahl (orange) and magnetic field (red) seen by the spacecraft. If this was a purely Alfvénic structure, then the spike would move away from the Sun in an antiparallel direction to **B** at the local Alfvén speed, C_A. In the frame of the spike, the shape of the structure would be static, with plasma flowing in along field lines on the upper left and through the spike and emerging at the lower right, always flowing at C_A. In the frame of the spacecraft, the constant flow along field lines in the propagating spike frame would translate into a radial increase of V by C_A when **B** is perpendicular to the R direction, and a maximum jump of $2C_A$ when **B** is completely inverted. Because the heat flux flows away from the Sun along magnetic field lines, it would rotate so as to always be antiparallel to **B** and appear locally to be flowing back to the Sun at the centre of this disturbance.